Astronomy & Astrophysics manuscript no. schaerer_cii_sfr_5
February 5, 2020

The ALPINE-ALMA [C II] survey

No or weak evolution in the [C II]–SFR relation over the last 13 Gyr

D. Schaerer[1,2], M. Ginolfi[1], M. Béthermin[3], Y. Fudamoto[1], P.A. Oesch[1], O. Le Fèvre[3], A. Faisst[4], P. Capak[4,27,28], P. Cassata[6,7], J.D. Silverman[8,32], Lin Yan[23], G.C. Jones[15,16], R. Amorin[12,13], S. Bardelli[11], M. Boquien[14], A. Cimatti[9,10], M. Dessauges-Zavadsky[1], M. Giavalisco[19], N.P. Hathi[17], S. Fujimoto[27,28], E. Ibar[20], A. Koekemoer[17], G. Lagache[3], B.C. Lemaux[5], F. Loiacono[9,11], R. Maiolino[15,16], D. Narayanan[27,30,31], L. Morselli[6,7], Hugo Méndez-Hernàndez[20], F. Pozzi[9], D. Riechers[29,22], M. Talia[9,11], S. Toft[27,28], L. Vallini[21], D. Vergani[11], G. Zamorani[11], and E. Zucca[11]

(Affiliations can be found after the references)

Received date; accepted date

ABSTRACT

The [C II] 158 μm line is one of the strongest IR emission lines, which has been shown to trace the star-formation rate (SFR) of galaxies in the nearby Universe and up to $z \sim 2$. Whether this is also the case at higher redshift and in the early Universe remains debated. The ALPINE survey, which targeted 118 star-forming galaxies at $4.4 < z < 5.9$, provides a new opportunity to examine this question with the first statistical dataset. Using the ALPINE data and earlier measurements from the literature we examine the relation between the [C II] luminosity and the SFR over the entire redshift range from $z \sim 4-8$. ALPINE galaxies, which are both detected in [C II] and dust continuum, show a good agreement with the local L([CII])–SFR relation. Galaxies undetected in the continuum with ALMA are found to be over-luminous in [C II], when the UV SFR is used. After accounting for dust-obscured star formation, by an amount SFR(IR)≈SFR(UV) on average, which results from two different stacking methods and SED fitting, the ALPINE galaxies show an L([CII])–SFR relation comparable to the local one. When [C II] non-detections are taken into account, the slope may be marginally steeper at high-z, although this is still somewhat uncertain. When compared in a homogeneous manner, the $z > 6$ [C II] measurements (detections and upper limits) do not behave very differently from the $z \sim 4-6$ data. We find a weak dependence of L([CII])/SFR on the Lyα equivalent width. Finally, we find that the ratio $L([CII])/L_{IR} \sim (1-3)\times10^{-3}$ for the ALPINE sources, comparable to that of "normal" galaxies at lower redshift. Our analysis, which includes the largest sample ($\sim$ 150 galaxies) of [C II] measurements at $z > 4$ available so far, suggests no or little evolution of the [C II]–SFR relation over the last 13 Gyr of cosmic time.

Key words. Galaxies: high redshift – Galaxies: evolution – Galaxies: formation – Galaxies: star formation

1. Introduction

The [C II] 158 μm line is an important coolant of the neutral interstellar medium (ISM), one of the strongest emission lines in the infrared (IR), which is also emitted relatively close to the peak of dust continuum emission. Although [C II] is long known to originate from HII regions, diffuse neutral and ionised ISM, and from photodissociation regions (e.g. Wolfire et al. 1995; Hollenbach & Tielens 1999), it has been found to trace star-formation. In particular, the [C II] luminosity has been shown to correlate well with the total star formation rate (SFR) of galaxies in our Galaxy, nearby galaxies, and up to $z \sim 2$ (see e.g. Pineda et al. 2014; de Looze et al. 2011; De Looze et al. 2014, and references therein).

Since [C II] 158 μm can be observed from the cosmic noon ($z \sim 2$) out to very high redshift ($z \sim 7-8$ Inoue et al. 2016) with ALMA, and potentially even into the cosmic dark ages with other facilities (cf. Carilli et al. 2017), this line has often been targeted, with the goal of using it as a probe of the ISM properties in distant galaxies, as a measure of the total SFR, unaffected by the possible presence of dust, and for other purposes, including redshift confirmation for galaxies in the epoch of reionization.

The first attempts to measure [C II] 158 μm in galaxies at $z > 6$ with ALMA have mostly been unsuccessful, yielding essentially non-detections, both for Lyα emitters (LAEs) and Lyman break galaxies (LBGs) (e.g. Ouchi et al. 2013; Ota et al. 2014; Maiolino et al. 2015). Subsequent observations, have detected [C II] in LAEs and LBGs both in blank fields and behind lensing clusters, finding several [C II]-underluminous galaxies at high-z and suggesting a large scatter in L([CII])-SFR (see e.g. Maiolino et al. 2015; Willott et al. 2015; Pentericci et al. 2016; Bradač et al. 2017; Carniani et al. 2018) compared to the local samples (De Looze et al. 2014). On the other hand Riechers et al. (2014) and Capak et al. (2015) successfully detected several $z \sim 5-6$ star-forming galaxies, revealing relatively broad [C II] lines and a good agreement with the local [C II]–SFR relation. Reanalysing the existing [C II] detections and non-detections of $z \sim 6-7$ galaxies, Matthee et al. (2019) have shown that the available data appears compatible with the De Looze et al. (2014) relation for SFR$\gtrsim 30$ M$_\odot$ yr^{-1} and may deviate from that for lower SFRs, if broader [C II] lines are assumed for the non-detections and the data are consistently compared. Conversely, using very similar data Harikane et al. (2018) and Harikane et al. (2019) conclude that $z = 5-9$ galaxies show a clear [C II]-deficit with respect to the local [C II]–SFR relation, and that this deficit increases with increasing Lyα equivalent width. Manifestly, no consensus has yet been reached on these questions, and it is unclear if the [C II] 158 μm line remains a good tracer of star-formation at $z > 4$ and if there is a quantitative change compared to the observations at low redshift.

To make progress on these issues, we use the ALMA Large Program to INvestigate C^+ at Early Times (ALPINE) survey, targeting 118 "normal" (i.e. main sequence) star-forming galaxies with known spectroscopic redshifts at $4.4 < z < 5.9$, and which is designed to provide the first statistical dataset allowing to determine the observational properties of [C II] emission at high-z. The survey has recently been completed and is described in detail in Le Fèvre et al. (2019), Béthermin et al. (2020), and Faisst et al. (2019). Our measurements, yielding 75 high significance detections of [C II] 158 μm and 43 non-detections, combined with the earlier [C II] observations of 36 galaxies at $z \sim 6-9.11$ from literature compilations, allow us to examine what is normal for high-z galaxies and shed new light on the above questions.

The paper is structured as follows. We briefly summarise the ALPINE [C II] dataset and other measurements in Sect. 2. We then examine the behaviour of the [C II] 158 μm luminosity with different SFR indicators, and we carefully compare the [C II]–SFR observations of high-z galaxies to the reference sample of De Looze et al. (2014) (Sect. 3). We combine the ALPINE dataset with the available [C II] observations at $z > 6$, and examine if all high-redshift observations show the same picture and if the [C II]–SFR relation is different in the early Universe (Sect. 3.3). Finally, we present the observed [C II]-to-IR ratio in Sect. 4. We discuss the possible caveats and future improvements in Sect. 5. Our main results are summarised in Sect. 6, and we provide results to fits to different datasets in the Appendix. We assume a ΛCDM cosmology with $\Omega_\Lambda = 0.7$, $\Omega_m = 0.3$, and $H_0 = 70$ km s^{-1} Mpc^{-1}, and a Chabrier IMF (Chabrier 2003).

2. Observations and derived quantities

The ALMA Large Program to INvestigate (ALPINE) survey, presented in Le Fèvre et al. (2019), has observed 118 "normal" star-forming galaxies with known spectroscopic redshifts at $4.4 < z < 5.9$. The ALPINE sample also includes 7 galaxies (HZ1, HZ2, HZ3, HZ4, HZ5, HZ6/LBG-1, and HZ8) that were previously observed with ALMA by Riechers et al. (2014) and Capak et al. (2015). It currently constitues the largest sample of [C II] observations at $z \sim 4-6$.

Details of the ALPINE data reduction and statistical source properties are described in Béthermin et al. (2020), from which we use the [C II] 158 μm line luminosities (L([CII]), 75 detections with high significance and 43 non-detections) and the dust continuum measurements (23 detections and 95 non-detections). The 158 μm rest-frame continuum fluxes have been converted to total IR luminosities, $L_{\rm IR}$, using an average empirically-based conversion from the 158 μm monochromatic continuum flux density to $L_{\rm IR}$ as described in Béthermin et al. (2020). The empirical template gives a conversion which is similar to a modified blackbody with a dust temperature of $T_d = 45$ K, a dust opacity at 850 μm of $k_{850} = 0.077$ m^2 kg^{-1} and a grey-body power-law exponent $\beta = 1.5$ (see e.g. Ota et al. 2014; Matthee et al. 2019).

For galaxies undetected in [C II] we use the aggressive 3σ upper limits of L([CII]) reported in Béthermin et al. (2020), defined as three times the RMS of the noise in velocity-integrated flux maps obtained collapsing a channel width of 300 km s^{-1} centered around the expected spectroscopic redshift. We then rescale these limits to reflect a more realistic (though less conservative) distribution of FWHM of our [C II]-undetected galaxies: motivated by the observed dependence of FWHM on L([CII]) shown in Fig. 2[1], we adopt FWHM = 150 km s^{-1}, less than the median of 252 km s^{-1} of the [C II]-detected ALPINE galaxies (Béthermin et al. (2020)) We note that, as discussed in Béthermin et al. (2020), by construction our 3 σ upper limits of L([CII]) can be underestimated if the sources are (i) just below the detection threshold, (ii) spatially extended (larger than the beam-size, e.g., $\gtrsim 1''$) and/or (iii) show very broad spectra (see e.g., Kohandel et al., 2019), where the two latter conditions are less likely to occur in less massive and less star forming objects.

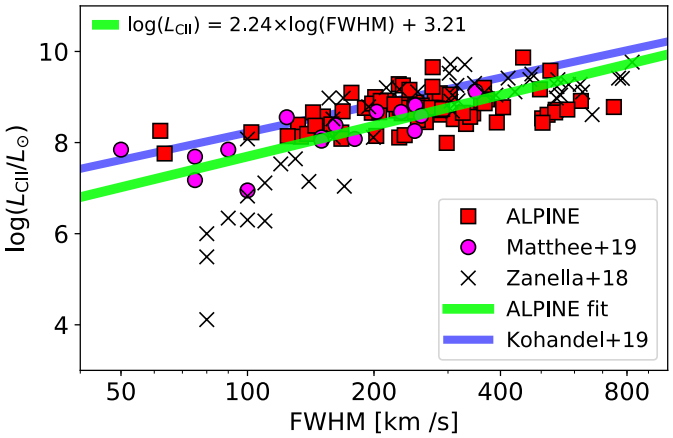

Fig. 1. Observed FWHM of the [C II] 158 μm line as function of the [C II] luminosity from ALPINE and other data from the literature (the compilation of $z > 6$ sources from Matthee et al. (2019) and available measurements for galaxies in the Zanella et al. (2018) compilation ($z \sim 0-6$). The violet dashed line is a "Tully-Fisher" like relation derived for high-z galaxies by Kohandel et al. (2019). The green solid line shows our best fit to the data.

For galaxies undetected in continuum we use aggressive upper limits determined by Béthermin et al. (2020), using the same conversion from158 μm rest-frame continuum fluxes to total IR luminosity. Finally, we also use $L_{\rm IR}$ values derived from the IRX–β relation obtained by stacking of the ALPINE sources, as described in Fudamoto et al. (2020). In absence of a direct detection of dust continuum emission, this is our preferred method to correct for dust-obscured star formation.

From the rich dataset of ancillary photometric and spectroscopic data, which is also available for the ALPINE sources (see Faisst et al. (2019) for details), we use the observed UV luminosity (or equivalently the absolute UV magnitude M_{1500} at 1500 Å). To compare our [C II] data with other measurements and results in the literature, we also use measurements of the Lyα equivalent widths, EW(Lyα), obtained from the rest-UV spectra of our sources, which were obtained during earlier spectroscopic observations with DEIMOS and VIMOS on the Keck and VLT telescopes. The spectra are discussed by Faisst et al. (2019); the Lyα measurements, available for 98 sources, are taken from Cassata et al. (2020), where a more detailed description of the Lyα properties is presented.

From the above-mentioned measurements of the UV and IR luminosities we derive three "classical" measures of star-formation rate, SFR(UV) uncorrected for attenuation, SFR(IR), and the total SFR(tot)=SFR(UV)+SFR(IR). We also use estimates of the total SFR, SFR(SED), obtained from the multi-band SED fits of Faisst et al. (2019). The different SFR measurements are all included in the ALPINE database (`https://cesam.lam.fr/a2c2s/`), where the data will be made public.

To allow a proper comparison of the L([CII])–SFR relation with the low-z galaxy sample of De Looze et al. (2014), we adopt

[1] A linear fit to the data yields $\log(L([\mathrm{CII}])/L_\odot) = 2.24 \times \log(\mathrm{FWHM}/(\mathrm{kms}^{-1}) + 3.21$.

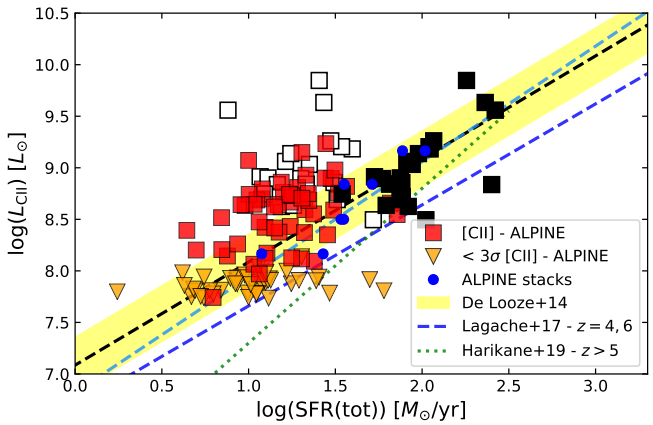

Fig. 2. [C II] as a function of the UV or UV+IR-derived SFR for the $z \sim 4.5$ ALPINE sources. Squares show the [C II] detections, orange triangles the 3 σ upper limits. Black squares show galaxies with continuum detection (SFR(UV)+SFR(IR) with filled squares; SFR(UV) only with open squares); red squares shows the SFR(UV) for the other ALPINE sources. Blue circles show the results from stacks of ALPINE sources in four bins of L([CII]) and two redshift bins, adapted from from Béthermin et al. (2020). The observations are compared to the [C II]-SFR relations of local galaxies determined by De Looze et al. (2014) adjusted to the Chabrier IMF by reducing the SFR by a factor of 1.06 (black dashed line), shown by the yellow band with a total width corresponding to 2σ. The green dotted line shows the relation fitted to observations of $z \sim 5$–9 galaxies by Harikane et al. (2019). The fits from the models of Lagache et al. (2018) for redshifts spanning the range of the observations are shown by the two blue dashed lines. Only the IR continuum-detected sources differ between the two panels, illustrating the importance of dust-obscured star formation in these galaxies.

the same conversion factors between $L_{\rm UV}$, $L_{\rm IR}$, and SFR as used in their paper. We note that the SFR(UV) calibration adopted by De Looze et al. (2014) agrees with the "classical" one from Kennicutt (1998), when rescaled to the same IMF. However, for the same IMF their IR calibration, taken from Murphy et al. (2011), yields SFR(IR) values larger by 30% (0.12 dex) than the Kennicutt (1998) calibration. Finally, we rescaled the SFR(UV) and SFR(IR) values by a factor of 1.06 from the Kroupa IMF (used by De Looze et al. (2014)) to the Chabrier IMF, for consistency with the other ALPINE papers[2] . Note that we assume SFR(IR)=0 per default and unless otherwise stated, for sources which are not detected in the continuum. This is discussed further below.

3. Relations between the [C II] 158 μm luminosity and SFR indicators at $z \sim 4 - 6$ and higher redshift

3.1. Comparing L([CII]) with UV, IR, and SED-fit based SFRs

As often done for high-z galaxies which are generally selected from the rest-UV and seldomly detected in the dust continuum, we first use a basic SFR indicator, SFR(UV) derived from the observed UV luminosity and which is available for the entire sample, to obtain the L([CII])–SFR relation shown in the left panel of Fig. 2. The ALPINE data is compared to the low-z HII-galaxy/starburst sample from De Looze et al. (2014) as a reference (henceforth named the "local" relation), which is often used in the literature. It includes 184 galaxies, shows a linear scaling between L([CII]) and SFR, and a scatter of 0.27 dex (see their Table 3)[3]. While the [C II] detections span a wide range between L([CII]) $\sim 5 \times 10^7$ L$_\odot$ and 5×10^9 L$_\odot$, SFR(UV) varies less, resulting thus in a relatively steep relation between L([CII]) and SFR(UV). Compared to the local L([CII])–SFR correlation the [C II] luminosity of our sources appears higher, in contrast to several high-z ($z \gtrsim 6$) galaxies where [C II] was found to be "underluminous", as mentioned in the introduction. More probably, the SFR is underestimated, as can be expected from dust-attenuation of the UV light.

To correct for dust attenuation in the simplest way, we plot in the same figure (Fig. 2) the [C II] measurements as a function of the total SFR, adding the dust-attenuated SFR(IR) to SFR(UV) for the galaxies for which we detect emission from the dust continuum. Clearly, for the continuum-detected sources the increase in SFR is significant, bringing them to fair agreement with the local L([CII])–SFR relation, as seen by the comparison with the left panel. This corresponds to galaxies with SFR(tot) $\gtrsim 30$ M$_\odot$ yr^{-1}.

On average, however, the [C II] luminosities of the 74 detected sources remain larger than expected from the local relation of De Looze et al. (2014), by a factor ~ 1.5 for the entire sample and a factor ~ 2 for the sources which are not detected in the continuum (red squares in Fig. 2). Approximately 40% of the [C II]-detected ALPINE galaxies are extended and classified as mergers from a morphological and kinematic analysis (Le Fèvre et al. (2019)). Excluding for example these mergers from the sample does not significantly change the deviation from the relation; on average a shift by a factor 1.25 in SFR(tot) remains, compared to a factor 1.5 shift for the entire sample. For the mergers alone the deviation is 0.28 dex, similar to that of several sources not detected in the continuum. From this we conclude that even if there were systematic differences between mergers and galaxies in the local sample, this would probably not explain the observed deviation between the ALPINE dataset and the De Looze et al. (2014) relation. Obscured star formation, below our current detection threshold in the ALMA measurements, is probably present in the majority of the ALPINE sample.

Béthermin et al. (2020) has carried out stacking of the ALPINE sources in different bins of [C II] luminosity, detecting thus the dust continuum in several of these bins and hence measuring in particular the *average* dust-attenuated contribution SFR(IR). After conversion to the same SFR calibrations used here (cf. above) their results are shown in Fig. 2. The ALPINE stacking results show a good agreement with the local [C II]–SFR relation, indicating that some correction for dust-obscured star formation is necessary even for the continuum un-detected galaxies and especially those at the low L([CII]) range.

Regrettably, the upper limits on the IR continuum fluxes of the *individual* ALPINE sources are sufficiently constraining. Even if we use the aggressive 1σ limits to determine a limit on hidden star-formation by summing SFR(UV) plus the SFR(IR) limit, we obtain the SFR(tot) limits shown in Fig. 3 (left), which are mostly in the range of SFR(tot)$\lesssim 40 - 100$ M$_\odot$ yr^{-1}. Clearly tighter constraints are desirable to examine if/how the high-z galaxies deviate or not from the local [C II]–SFR relation.

[2] In short, the final adopted SFR calibrations are: SFR(UV)/(M$_\odot$ yr^{-1})= $8.24 \times 10^{-29} L_\nu$, where L_ν is in units of ergs/s/Hz, or equivalently SFR(UV)/(M$_\odot$ yr^{-1})= $1.59 \times 10^{-10} L_{\rm UV}/L_\odot$, where $L_{\rm UV}$ is calculated at 1500 Å. And SFR(IR)/(M$_\odot$ yr^{-1})= $1.40 \times 10^{-10} L_{\rm IR}/L_\odot$.

[3] For comparison, their entire sample with 530 galaxies, shows a larger scatter (0.42 dex) and a [C II] 158 μm luminosity which is lower by 0.07 dex for a given SFR.

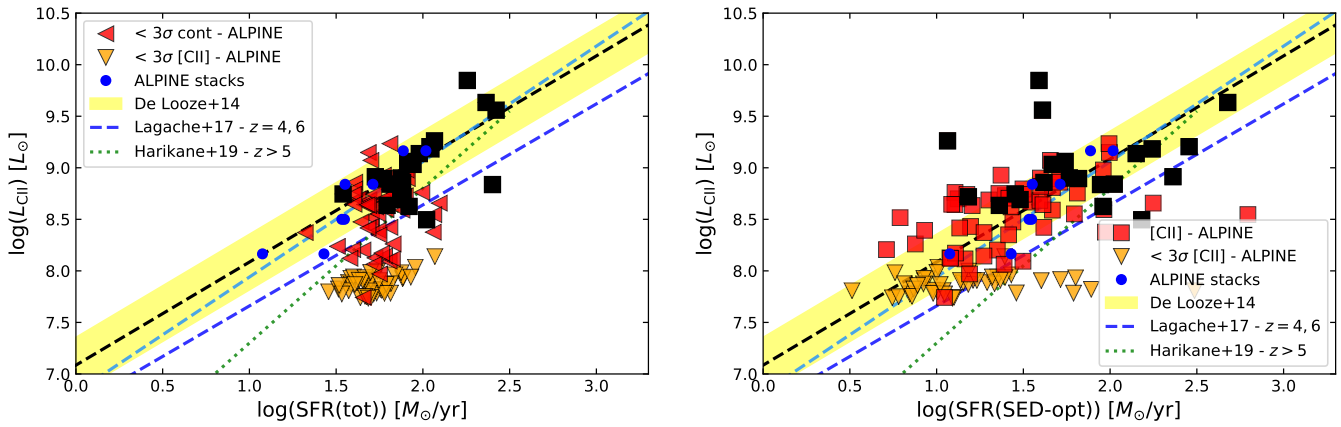

Fig. 3. Same as Fig. 2. *Left:* SFR(UV+IR) where the IR contribution now includes the 1-σ limit on $L_{\rm IR}$. *Right:* Using the SFR derived from SED fitting of the stellar emission (rest-UV to optical).

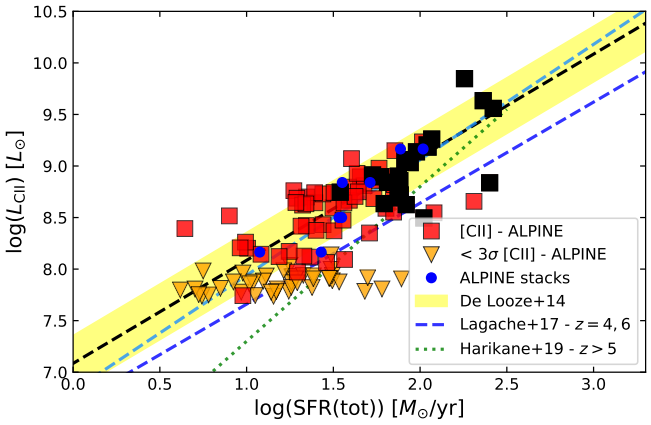

Fig. 4. Same as Fig. 2 using SFR(UV+IR). Here SFR(IR) is derived from the observed UV slope and luminosity using the ALPINE IRX-β relation obtained from stacking (Fudamoto et al., in prep.). The [C II]-detected galaxies follow well the local relation.

SED fitting provides one way to account for this. Using the results from the multi-band SED fitting results discussed in Faisst et al. (2019) and assuming a Calzetti attenuation law, reduces the apparent [C II] excess found when not accounting for dust-obscured star formation. Indeed, as shown in Fig. 3 (right), the mean offset between the local L([CII])–SFR relation and the ALPINE data ([C II] detections only) is then reduced to 0.06 dex, although the scatter around the local relation is quite large (0.40 dex). However, we note that a comparison using SED-based SFR values with the relations established by De Looze et al. (2014) would be methodologically inconsistent, since these authors use simple (UV and IR) SFR calibrations, whereas SED fitting allows for varying star-formation histories, different ages etc., which may not yield compatible results and is known to give a larger scatter (see e.g. Wuyts et al. 2011; Schaerer et al. 2013). In any case, all the methods illustrated here show that most, if not all of the $z \sim 4-6$ galaxies included in the ALPINE sample must suffer from some dust attenuation.

3.2. The [C II]–SFR relation accounting for hidden SF in $z \sim 4-6$ galaxies

We now proceed to account for hidden SF in all individual ALPINE galaxies in the best possible and consistent way to compare the [C II]–SFR relation with lower redshift data. To do this we use the average IRX–β relation derived by Fudamoto et al. (2020) for the ALPINE sample from median stacking of the continuum images in bins of the UV slope β. These authors found an IRX–β relation, which is close to but below the relation expected for the SMC attenuation law, with little evolution across the redshift range of the ALPINE sample. We apply their mean IRX–β relations to each individual source for which the dust continuum has not been detected, yielding thus a predicted $L_{\rm IR}$, and hence a corresponding SFR(IR), using the same assumptions as for the rest of the sample. For continuum-detected galaxies we use the standard SFR(IR) values, shown above.

The result is illustrated in Fig. 4, showing a very small offset from the local relation (−0.02 dex) and a scatter of 0.28 dex around it (for the [C II] detections). In other words, taking into account a relatively small correction for hidden SF, which is compatible with our continuum non-detections and the IRX–β relation, the ALPINE [C II]-detected galaxies nicely follow the same L([CII])–SFR relation as low-redshift galaxies.

Now, if we include the "agressive" [C II] non-detections and fit the data with a linear relation of the form

$$\log(L([\mathrm{CII}])/L_\odot) = a + b \times \log(\mathrm{SFR}/M_\odot \mathrm{yr}^{-1}) \quad (1)$$

using a Bayesian fit including censored data[4], we obtain a slope which is marginally steeper than the local relation (1.17 ± 0.12, the results from different fits are given in the Appendix). However, adopting more conservative upper limits for L([CII]), e.g. the "secure" limits[5] from Béthermin et al. (2020), which are typically a factor 2 less deep, our fits including censored data yields a slope of 0.99 ± 0.09, compatible with unity, and slightly offset (by ~ -0.11 dex) with respect to the local relation. From this we conclude that main sequence galaxies at $z \sim 4-6$ may

[4] We follow the method of Kelly (2007) implemented in the python package *linmix*, `https://github.com/jmeyers314/linmix`. The method allows for uncertainties in one quantity, here L([CII]).

[5] "Secure" limits have been calculated by summing the 3 σ rms of the noise to the highest flux measured in 1 arcsec around the phase center in visibility-tapered velocity-integrated flux maps (see Béthermin et al. (2020) for more details).

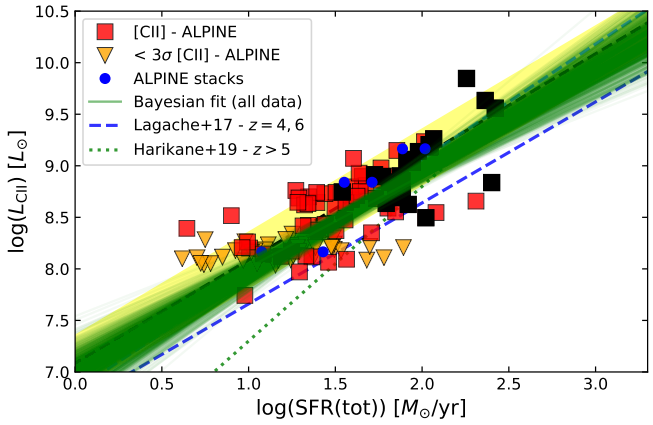

Fig. 5. Same as Fig. 4 for ALPINE sources, but adopting conservative upper limits for the [C II] non-detections (2 times the agressive 3σ upper limits). The Bayesian linear fit to all the measurements (detections and upper limits) is shown by the dark green lines/band which also illustrates the probability distribution of the fit. The fit yields a slope of 0.99 ± 0.09, compatible with unity, and a small but insignificant offset (by ~ -0.05 dex) with respect to the local relation.

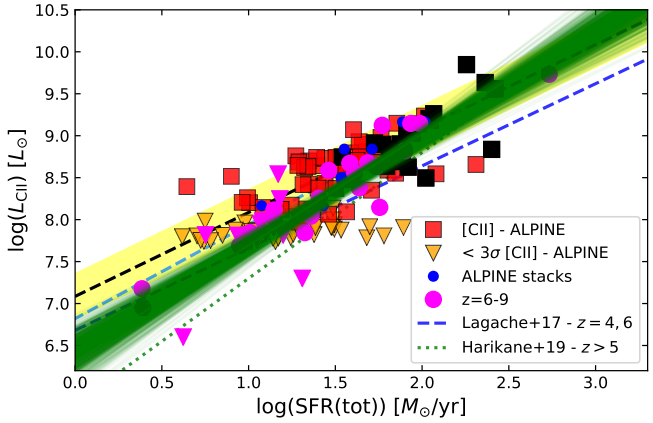

Fig. 6. [C II]–SFR relation combining the ALPINE sample and observations of $z \sim 6-9$ galaxies taken from the literature. The $z > 6$ data, after properly uniformisation, is plotted with pink symbols. The SFR of all sources includes an SFR(IR) contribution, determined from the observed dust continuum or from the IRX–β relation if undetected. All [C II] non-detections are shown as 3σ (aggressive) upper limits. The Bayesian linear fit to all the $z > 4$ measurements (detections and upper limits) is shown by the dark green lines/band; the slope is somewhat steeper than unity, 1.26 ± 0.10.

show the same L([CII])–SFR relation as low redshift galaxies or a relation which is somewhat steeper (with an exponent $\sim$ 1.2). More firm statements are difficult to make at the present stage, until [C II] non-detections and the exact amount of dust-obscured star-formation are better quantified.

3.3. A universal behaviour of L([CII]) at $z > 4$?

We now examine how the ALPINE [C II] measurements of $z \sim 4-6$ galaxies compare with the other available observations at even higher redshifts. To do this we use the recent compilation of Matthee et al. (2019), which includes 25 reported ALMA [C II] observations of galaxies with known spectroscopic redshifts between $z = 6.0$ and $z = 7.212$. Importantly, Matthee

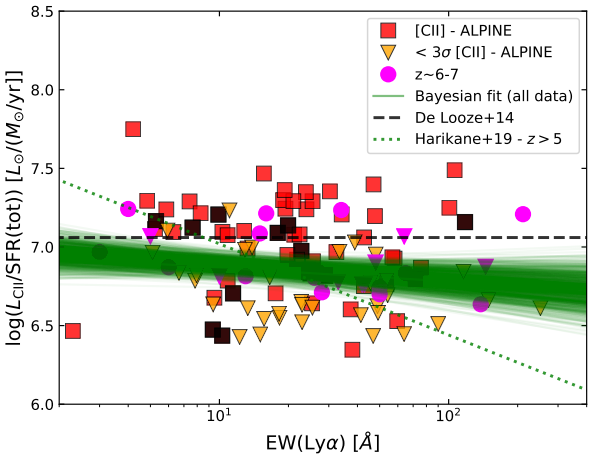

Fig. 7. L([CII])/SFR(tot) as a function of the rest-frame Lyα equivalent width of the ALPINE sources and $z \sim 6-7$ galaxies taken from the literature (pink symbols). The dotted line shows the fitting relation obtained by Harikane et al. (2018) for a compilation of $z \sim 5.7-7$ galaxies, the horizontal line the average value from the local relation. The green lines/band shows the fit to the data; the resulting slope is -0.10 ± 0.06, indicating a weak dependence on EW(Lyα).

et al. (2019) have recomputed [C II] non-detection limits using empirically-motivated [C II] line widths[6]. Furthermore they have uniformly re-derived SFR(UV) and SFR(IR) from the observations, assuming a modified blackbody with $T_d = 45$ K. We use their derived properties, after rescaling them to the IMF and SFR(IR) calibrations adopted in this paper (see Sect. 2). To this we add 11 measurements (6 detections, 5 upper limits) of galaxies between $z = 6.0$ and 9.11 from Harikane et al. (2019), who report 3 new observations and 8 others not included in the Matthee et al. (2019) compilation. For consistency, we use the SFR(UV) and SFR(IR) values, and we carefully rescale their results to a single, consistent IMF and to the same SFR(IR) calibration. Finally, for sources which are not detected in the dust continuum, we correct for hidden SF by applying the IRX–β relation derived at $z \sim 5.5$ from the ALPINE sample, when the UV slope is reported. For the majority of the galaxies the correction turns out to be small, since their UV slope is fairly blue. The data is plotted Fig. 5.

Clearly, most of the known $z \gtrsim 6$ galaxies follow largely the same behaviour/trend as the ALPINE galaxies. At SFR(tot)$\gtrsim$ 30M$_\odot$ yr^{-1} very few points deviate by more than 1σ from the De Looze et al. (2014) relation. Differences between our results and those shown in Harikane et al. (2019) are explained by several effects: by our use of a single IMF consistent with the De Looze et al. (2014) relation, a consistent use of calibrated SFR determinations for all sources (no SED-based SFR as for some of their sources) following Matthee et al. (2019), and finally by the adoption of conservative line widths to determine upper limits on L([CII]).

[C II] is undetected in a significant number of galaxies at SFR$\lesssim$ 30M$_\odot$ yr^{-1}. Assuming a FHWM= 150 km s^{-1} for the ALPINE sources and the 15 upper limits from the $z > 6$ data discussed above, we find that the deepest 3σ upper limits are $\log(L([\mathrm{CII}])/L_\odot) < 7.8$ for the bulk of the data. While a fraction

[6] They use FWHM= $-1215 - 66 \times M_{\mathrm{UV}}$ km s^{-1}, translating to a minimum FWHM= 123 km s^{-1} for the UV-faintest [C II] non-detected galaxy in their sample (Matthee, private communication).

of those are well within the scatter around the "local" De Looze et al. (2014) relation, several are probably below this, which pushes the average L([CII])/SFR ratio of both the ALPINE sample and the full high-z galaxy sample to $\log(L([CII])/)SFR \approx 6.85$ $L_\odot/M_\odot$ yr^{-1}, approximately 0.2 (0.1) dex lower than the reference value from De Looze et al. (2014) for the HII/starburst (complete) galaxy samples (see also Fig. 7). Two non-detections at SFR$< 30 M_\odot$ yr^{-1} are strongly underluminous in [C II] compared to the rest of the sample: these are two lensed galaxies at $z > 8$, A2744-YD4 at $z = 8.382$ and MACS1149-JD1 at $z = 9.11$ observed by Laporte et al. (2019), and which were previously detected by ALMA in the [O III] 88μm line by Laporte et al. (2017) and Hashimoto et al. (2018). On the other hand, another [O III]-detected lensed $z = 8.312$ galaxy (MACS0416-Y1 from Tamura et al. 2019) is detected in [C II] and follows well the observed trend.

To quantify again this behaviour we use the Bayesian fit including censored data. The results including the uncertainties and upper limits on L([CII]) are shown by the green lines/band in Fig. 3.2. The fit shows, that the inclusion of the upper limits primarily, leads to a somewhat steeper (super-linear) slope (1.26 ± 0.1) in the L([CII])–SFR relation for galaxies at $z > 4$ and to an overall, but slight decrease of the normalisation, i.e. to a lower [C II] luminosity on average at a given SFR, as already mentioned and also shown in Fig. 7. Overall, the observational data shows a behaviour, which is quite comparable to the mean L([CII])–SFR relations predicted by the models of Lagache et al. (2018) between $z = 4$ and $z = 6$. The fit to the data shown in Fig. 3.2 is also similar to the mean relation obtained from the recent simulations of high-z galaxies by Arata et al. (2020), who find a somewhat steeper slope of 1.47.

Interestingly, with the enlarged sample (ALPINE + $z > 6$ galaxies) our fits yield slopes steeper than unity using both options for the [C II] upper limits (agressive versus conservative; cf. above). This result is mostly driven by few additional data points at low L([CII]) and low SFR, which have low uncertainties on L([CII]) and thus a fairly strong leverage. Whether these points are truly representative of the bulk of the population of fainter galaxies or "outliers" remains to be confirmed with new observations probing this regime.

Overall, we conclude that the [C II] measurements (detections and upper limits) of star-forming galaxies at $z \sim 4-8$ follow quite well a unique relation between L([CII]) and SFR(UV)+SFR(IR) over nearly 2 orders of magnitude in the [C II] luminosity. This holds for a wide variety of galaxy types (LAEs, LBGs primarily, plus two SMGs from Marrone et al. (2018) included in the Harikane et al. (2019) compilation) issued from different selections. Taking the [C II] non-detections into account the L([CII])–SFR rrelation appears to be somewhat steeper and offset from the "local" counterpart determined by De Looze et al. (2014). Whether the relation shows a turnover below SFR$\lesssim 10-30$ $M_\odot$ yr^{-1}, as suggested e.g. by Matthee et al. (2019), cannot be established from the available data. This would require more sensitive measurements.

3.4. Is there a dependence of [C II] with the Lyα equivalent width in high-z galaxies ?

Several authors have pointed out that galaxies with an increasing Lyα equivalent width show a fainter [C II] emission, compared to expectations from the local [C II]-SFR relation (see e.g. Carniani et al. 2018; Harikane et al. 2018; Harikane et al. 2019). Benefitting now from the large amount of new data from ALPINE for which we also have EW(Lyα) measurements (for 58 [C II]-detected plus 33 non-detected sources, taken from Cassata et al. (2020)), we show the behaviour of L([CII])/SFR(tot) as a function of EW(Lyα) in Fig. 7. The ALPINE sources cover a wide range of Lyα equivalent widths, including also relatively large EWs, some of which were selected as LAE. Again a large scatter is found in L([CII])/SFR at all values of EW(Lyα), and the fit to all the data including the non-detections shows a weak dependence of EW(Lyα) on L([CII])/SFR[7]. Clearly, we cannot claim a strong anti-correlation of [C II] with increasing Lyα equivalence width, in contrast to Harikane et al. (2019). The difference with their work comes from our significantly larger dataset, our use of "uniformised" values for SFR, and the use of a more conservative line width for the determination of the upper limits on [C II] luminosities, as already mentioned above.

4. Observed [C II] 158 μm line to IR continuum ratios

With the exception of some lensed sources from the SPT survey (Gullberg et al. 2015), the $z > 3$ galaxies currently detected in the dust continuum have typical (lensing-corrected, if applicable) IR luminosities in the range of $L_{IR} \gtrsim 10^{11}$ to 2×10^{12} $L_\odot$, hence are LIRG or ULIRG by definition. This is also the case for the continuum-detected ALPINE sources (see Béthermin et al. (2020)). In this regime of high IR luminosities low-z galaxies show the well-known "[C II]-deficit", i.e. a drop of $L([CII])/L_{IR}$ towards high L_{IR} (see e.g. Malhotra et al. 2001; Graciá-Carpio et al. 2011). It is therefore of interest to examine how high redshift galaxies, the ALPINE sample in particular and others, behave in this respect.

Since the IR continuum is undetected in many observations of normal star-forming galaxies at high redshift, we first plot the $L([CII])/L_{IR}$ ratio as a function of the [C II] luminosity instead of L_{IR}. The result is shown in the left panel of Fig. 8, where we show the data for all the [C II]-detected galaxies of ALPINE, the $z > 6$ data from the compilation of Matthee et al. (2019), other [C II]-detections (non-AGN-dominated sources) at $z > 3$ taken from the compilation in Gullberg et al. (2015), the SPT sources of Gullberg et al. (2015), and observations at $z < 3$ from the compilation of Zanella et al. (2018). Note that we use the total IR luminosity here (from 8-1000 μm), following e.g. Zanella et al. (2018), whereas other authors use the far-IR luminosity, L_{FIR} (from 40-122 μm restframe), as a reference; in the Zanella et al. (2018) compilation one typically has $L_{IR}/L_{FIR} = 1.6$. For the SED template used for ALPINE, $L_{IR}/L_{FIR} = 1.628$.

The ALPINE sources detected in the continuum show a ratio $L([CII])/L_{IR} \sim (1-3) \times 10^{-3}$ (or a factor of 1.628 higher when compared to L_{FIR}), comparable to the "normal" $z < 1$ sources, whereas the IR luminous [C II]-deficient galaxies have $L([CII])/L_{IR} < 10^{-3}$. The same is also found for the other continuum-detected $z > 6$ galaxies, and the majority of the $z \sim 4-7$ sources which are currently undetected in the dust continuum are also compatible with normal or higher $L([CII])/L_{IR}$ ratios. In other words, the majority of the $z > 4$ galaxies where [C II] is detected do not seem to show a deficit in $L([CII])/L_{IR}$, similar to earlier findings at lower redshift (e.g. $z \sim 1-2$, Zanella et al. 2018). On the other hand, the SPT sample, which is significantly brighter than the ALPINE sources and $z > 6$ LBGs and LAEs, shows several sources with $L([CII])/L_{IR} < 10^{-3}$ and an increasing [C II]-deficit at IR luminosities above $\gtrsim 10^{12}$ $L_\odot$,

[7] The Bayesian fit yields $\log(L([CII])/SFR) = (6.99 \pm 0.07) - (0.10 \pm 0.06) \times \log(EW)$ in the units plotted in Fig. 7.

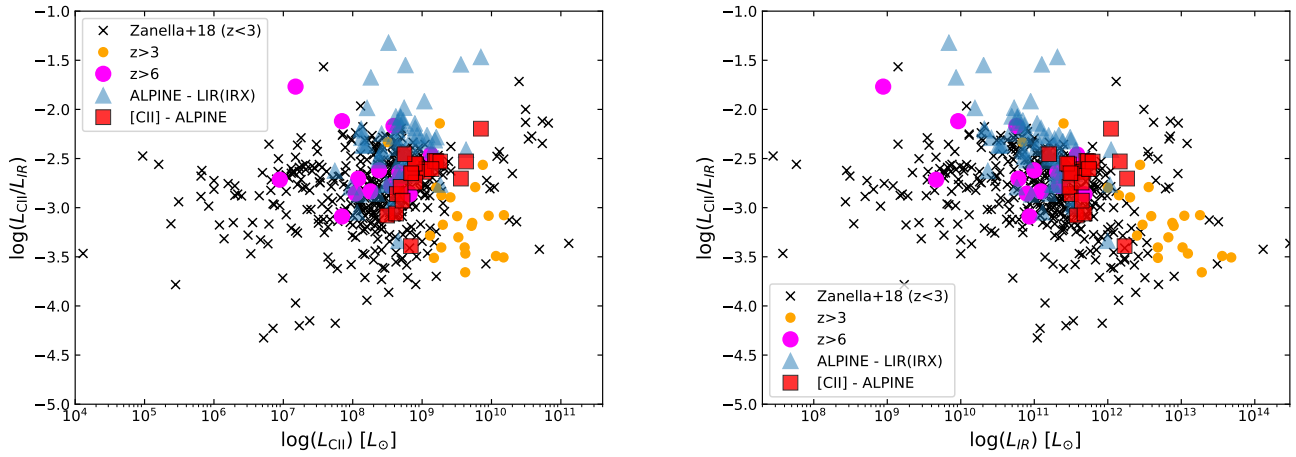

Fig. 8. L([CII])/$L_{\rm IR}$ versus L([CII]) (left panel) and $L_{\rm IR}$ (right) for the ALPINE sources and comparison samples where the [C II] line is detected. Lower limits (shown by triangles) correspond to 3σ limits on $L_{\rm IR}$. For the $z > 6$ sources, taken from the Matthee et al. (2019) sample, we adopt $T_d = 45$ K for the detections and $L_{\rm IR}$ upper limits. For galaxies not detected in the dust-continuum we show their L([CII])/$L_{\rm IR}$ lower limit in the left panel. In the right panel the $L_{\rm IR}$ limits have been replaced by the $L_{\rm IR}$ values computed from the IRX–β relation, where possible.

as shown by Gullberg et al. (2015). One may therefore speculate that a [C II]-deficit is also present in high-z galaxies, albeit at intrinsically higher IR luminosities, again suggesting that the [C II]/IR-deficit is not a universal property, as already suggested earlier (cf. Zanella et al. 2018).

In the right panel of Fig. 8 we show a more classical version of the dependence of the L([CII])/$L_{\rm IR}$ratio, plotted as a function of $L_{\rm IR}$, where the IR luminosity of the high-z ($z \sim 4-6$ galaxies from ALPINE and the $z > 6$ sample) is taken from the observations or has been computed from the ALPINE IRX–β relation (as used in Figs. 4–7) for the continuum non-detected sources. Most of the latter sources have predicted $L_{\rm IR} \sim 10^{10} - (3 \times 10^{11})$ L$_\odot$, and L([CII])/$L_{\rm IR}$ ratio ranges between 10^{-3} and 10^{-2}, compatible with the bulk of the $z < 3$ galaxies.

Since the observed decrease of L([CII])/$L_{\rm IR}$ in low and high-z galaxies is known to correlate with the increasing dust temperature (e.g. Malhotra et al. 2001; Graciá-Carpio et al. 2011; Diaz-Santos et al. 2013; Gullberg et al. 2015), one might be tempted to conclude that the "normal" L([CII])/$L_{\rm IR}$ ratio found for the majority of the ALPINE galaxies and $z > 6$ LBGs and LAEs, could indicate that these sources do not harbor particularly hot dust. In the context of the intensely-debated uncertainties on the typical dust temperatures of normal galaxies in the early Universe (see e.g. Bouwens et al. 2016; Faisst et al. 2017; Ferrara et al. 2017) this would have important implications. However, Fig. 3.4 should not be over-interpreted since the inferred IR luminosity depends itself on the assumed IR SED template, i.e. directly or indirectly on T_d. Independent constraints on the IR SED and dust temperature of high-z galaxies are clearly needed.

5. Discussion

If star-formation was unobscured in most of the $z \sim 4-6$ galaxies covered by the ALPINE survey, our observations would indicate that [C II] is over-luminous at a given SFR≈SFR(UV), compared to the observed correlation for low redshift galaxies (see Fig. 2). At face value, such a conclusion would be quite in contrast with earlier studies of, e.g., $z > 6$ galaxies, which have argued that [C II] was less luminous than expected from comparisons with the low-z reference sample (see e.g. Ouchi et al. 2013; Bradač et al. 2017; Harikane et al. 2018).

However, as argued above, it seems much more likely that a fraction of the UV light from star-formation is attenuated by dust, in the majority of our targets, i.e. also in those from which we do not detect dust continuum emission with ALMA. Indeed, a relatively small correction of SFR(UV) – upward by a factor ~ 2 on average – is sufficient to bring the [C II] measurements on average into agreement with the local L([CII])–SFR relation (cf. Sect. 3.2). The amount of this correction appears very reasonable from several points of view: first it corresponds to the average correction obtained from multi-band SED fitting of the rest-UV-to-optical SED, and second, the same correction is found on average from applying an empirically–calibrated IRX–β relation of the ALPINE galaxies derived from stacking to the individual ALPINE galaxies, which are not detected in the dust continuum. Finally, stacking the continuum in bins of L([CII]) also indicates a necessary correction to the SFR(UV) as shown by Béthermin et al. (2020), leading to a fair agreement of the stacked data with the local relation.

Taking into account a correction for dust-obscured star formation, we have then examined and derived the empirical relation between L([CII]) and the total SFR(tot) for $z > 4$ galaxies, using both the ALPINE sample covering $z \sim 4-6$ and data from the literature for $z \sim 6-9$ galaxies, and including also [C II] non-detections in a Bayesian linear fit of the data (Sect. 3.3 and Appendix). We have also stressed the importance of a consistent use of SFR calibrations, IMF normalisations, and empirically-motivated [C II] line widths to compute upper limits (see also Matthee et al. 2019), which must be taken into account for meaningful and consistent comparisons of different data sets and to establish, e.g., a possible evolution of the L([CII])–SFR relation with redshift. Some of our results are obviously also subject to uncertainties and future improvements, which we now briefly discuss.

5.1. Caveats and future improvements

Making reasonable assumptions on the dust-obscured SFR and using for the first time a large sample of up to 150 galaxies, we

have shown that the [C II] luminosity of high-z ($z > 4$) galaxies correlates well with the total SFR, over approximately 2 orders of magnitude in SFR. The data is well described by a linear relationship between $\log(L([\mathrm{CII}]))$ and $\log(\mathrm{SFR_{tot}})$ with a slope close to unity ($b \sim 0.8 - 1.3$) (see Table A.1). However, the exact slope of the relation depends in part on the [C II]-undetected sources and hence on the detailed assumptions on the upper limits, which depends not only on assumed line widths, but also on the hypothesis about size (point-like or slightly extended sources). Deeper data for some of the ALPINE targets would easily be possible with ALMA, and helpful to better understand the sources with $\log(L([\mathrm{CII}])) \lesssim 10^8$ L$_\odot$. To firm up the result of a possibly steeper L([CII])–SFR relation at high-z than for local galaxies it is also clearly important to acquire more measurements of fainter galaxies with lower star formation rates, ideally at SFR $\lesssim 1 - 3$ M$_\odot$ yr^{-1}, where currently only very few observations of lensed galaxies have been obtained (Knudsen et al. 2016; Bradač et al. 2017).

Although we fit the available data with simple linear relations (i.e. a power-law dependence of L([CII]) on SFR), nature may be more complicated and the conditions different in high redshift galaxies. The high-z data discussed here does not allow us to exclude a different behaviour at low SFR or low L([CII]), as suggested e.g. by Matthee et al. (2019). However, on resolved scales in our Galaxy and for individual galaxies from the nearby Universe up to $z \sim 1-3$, different studies have empirically established a correlation between [C II] and the total SFR with simple power laws with exponents of $\sim 0.8-1.2$ extending over approximately 6 orders of magnitudes (see e.g. Pineda et al. 2014; de Looze et al. 2011; De Looze et al. 2014; Zanella et al. 2018), and which includes the range probed by high-z observations. From an empirical point of view and in absence of strongly deviating data we therefore do not consider other functional forms of the [C II]–SFR relation.

Beyond [C II], the second fundamental quantity for this work is obviously the total SFR, which is currently not trivial to determine, due to technical limitations (insufficient sensitivity to detect dust continuum emission) and to our limited knowledge of the dust properties and IR template, which are required to infer the total IR luminosity, and hence the dust-obscured part SFR(IR). On the other hand, SFR(UV) is trivial to determine for the galaxies of interest here, since all of them where previously detected at these wavelengths for our survey (Le Fèvre et al. (2019)). The IR template used in our work to translate the rest-frame 158 μm continuum measurements to the total L_{IR} has a similar "bolometric correction" as a modified blackbody (MBB) with $T_d \approx 42$ K (Béthermin et al. (2020)). Using, e.g., the empirical template of Schreiber et al. (2018) would imply L_{IR} values higher by 43%, comparable to a MBB with $T_d \sim 45$ K. If even higher dust temperatures were appropriate, L_{IR} would, e.g., increase by a factor 1.87 (3.79) for $T_d = 50$ (60) K compared to (Béthermin et al. (2020)).

With our assumptions and the adopted IRX–β correction, for the ALPINE galaxies one has SFR(UV) $\approx$ SFR(IR) on average, and most galaxies have SFR(UV) $\lesssim 2$ SFR(IR). In this case, an increase of L_{IR} by a factor 2 (3) would translate to an increase of the total SFR by a factor 1.5–1.6 (2–2.3). This effect could thus shift the [C II]–SFR relation by this amount, away from the local relation. If, and by how much this could also change the slope of the relation, depends if the dust-obscured SFR fraction is constant in all galaxies, and how the dust temperature may vary with galaxy properties, all of which are largely unknown for high-z galaxies.

Clearly, determining accurately the total SFR of high-z galaxies will lead to significantly more robust results on the [C II]–SFR relation in the distant Universe. Efforts are under way to constrain the dust temperatures at high-z (e.g. Hirashita et al. 2017; Faisst et al. 2017; Bakx et al. 2020). Alternatively, the JWST should soon provide measurements of rest-optical lines including Hydrogen recombination lines, which will allow one to determine, e.g., the Hα SFR and dust-corrections using the Balmer decrement for high-z galaxies. This could become an important and complementary method to nail down some of the uncertainties discussed here, and indirectly also to constrain the dust temperature and L_{IR} of distant galaxies.

Finally, we would like to caution that the [C II] luminosity may not necessarily trace accurately the SFR in general, as especially in high redshift galaxies. Indeed, although empirically L([CII]) correlates well with the SFR, the main physical reason(s) for this dependence are not well understood and predictive models are therefore difficult to construct, presumably largely since [C II] is known to originate from a broad range of ISM phases and regions with different conditions (see e.g. Vallini et al. 2015; Lagache et al. 2018; Ferrara et al. 2019; Popping et al. 2019). In fact, the empirical correlations of L([CII]) determined here and in earlier studies are with the UV+IR luminosity, or a combination of the two, which can be converted to the SFR if one assumes a certain star formation history and age of the population. More fundamentally, the data is therefore probably indicating a correlation of the [C II] luminosity with the intrinsic UV luminosity of the galaxy – part of which emerges in the UV and the other part after processing by dust in the IR – which is also physically meaningful, since [C II] requires photons capable of singly ionizing carbon atoms, i.e. with energies > 11.26 eV (wavelength < 1102 Å). This implies in particular that L([CII]) does not need to follow closely the instantaneous SFR in galaxies with strongly varying (irregular, burst etc.) star-formation histories, where significant variations between L_{UV} and the SFR are expected (see e.g. Schaerer et al. 2013; Madau & Dickinson 2014). Such situations are probably more common in the early Universe, and one may therefore expect a better correlation of L([CII]) with the intrinsic (total) UV luminosity than with other tracers of the SFR, such as H recombination lines.

6. Conclusions

We have analysed the new [C II] 158 μm measurements from the ALPINE survey of star-forming galaxies at $z \sim 4 - 6$ (Le Fèvre et al. (2019), Béthermin et al. (2020), Faisst et al. (2019)), which provides for the first time a large sample (118 galaxies) to study [C II] emission and its correlation with the star formation rate at high redshift. We have examined whether our data and other observations at $z > 6$ – totalling now 153 galaxies – are compatible with the observed correlation between the [C II] luminosity and SFR found at lower redshift, and described in the De Looze et al. (2014) reference sample.

To compare the high-z observations to the earlier data, we have used consistent SFR calibrations (based on UV and IR continuum luminosities) and a carefully homogenized IMF. We have also taken into account the [C II] non-detections, which are translated into upper limits on L([CII]) assuming empirically-motivated assumptions on the [C II] line widths, which we re-examined using our and literature data (see Fig. 1).

The ALPINE galaxies, which are both detected in [C II] and the dust continuum, show a good agreement with the low-z L([CII])–SFR relation. A fraction of the ALPINE galaxies which are non-detected in the dust continuum appear over-luminous

in L([CII]) compared to expectations from the De Looze et al. (2014) relation, when no correction for dust attenuation is made (see Fig. 2 left). This is in contrast with earlier studies which have often reported apparent deficits of [C II] in high-z galaxies (e.g. Ouchi et al. 2013; Inoue et al. 2016; Harikane et al. 2018). Using the results from two different stacking methods, described in Béthermin et al. (2020) and Fudamoto et al. (2020), and SED fits, allows us to account for dust-obscured star formation in these galaxies, increasing thus their total SFR by a factor ~ 2 on average, which brings the ALPINE galaxies in agreement with the local [C II]–SFR relation (Figs. 3 right and 4).

When conservative upper limits from the [C II] non-detected galaxies ($\sim 1/3$ of the ALPINE survey) are also considered, we find that L([CII]) scales linearly with the total SFR for the ALPINE sample, although with a slightly lower normalisation (L([CII])) than the local HII/starburst galaxy sample of De Looze et al. (2014). Using more agressive upper limits leads to a steepening of the L([CII])–SFR relation. A steeper increase of L([CII]) with SFR is also found when all the available [C II] measurements (detections and upper limits) at $z \sim 4-8$, including other ALMA measurements from the literature are combined (Fig. 6). Given the remaining uncertainties on the [C II] non-detected galaxies and the exact amount of dust-obscured SFR, we conclude that the exact slope of the L([CII])–SFR relation at $z > 4$ is not firmly established.

Analysing the homogenised sample of 153 $z > 4$ galaxies with [C II] measurements (detections or upper limits) we found that very few galaxies deviate significantly from the bulk of the sample and that most $z \sim 4-8$ galaxies show an L([CII])–SFR relation which is not very different from that of low-z galaxies nearly 13 Gyr later. In other words the currently available data show no strong evidence for a deficit of [C II] from $z \sim 4$ to 8, in contrast to several earlier results, but in line with other suggestions (Carniani et al. 2018; Matthee et al. 2019). The only strong outliers from the L([CII])–SFR relation are two galaxies at $z > 8$ with [O III] 88μm line detections with ALMA and no [C II] 158 μm (Laporte et al. 2019), which may indicate a more fundamental change of properties in the very early Universe.

We have also examined the behaviour of L([CII])/SFR with the observed Lyα equivalent width of the ALPINE galaxies and literature data, and we do not find a strong dependence of the [C II] excess or deficiency with EW(Lyα) at $z > 4$ (Fig. 7), in contrast with earlier suggestions (e.g. Harikane et al. 2018; Harikane et al. 2019; Matthee et al. 2019). Finally, we have shown that the derived ratio $L([\mathrm{CII}])/L_{\mathrm{IR}} \sim (1-3) \times 10^{-3}$ for the ALPINE sources, comparable to that of "normal" galaxies at lower redshift (Fig. 8).

Overall, our results, using 153 galaxies at $z > 4$, suggest that the [C II] luminosity can be used to trace the SFR at these high redshifts, although the scatter is higher than at low redshift, as already hinted at e.g. by Carniani et al. (2018). Furthermore, there is some evidence for a possible steepening of the L([CII])–SFR relation compared to $z < 3$, although this needs to be firmed up with future measurements and better constraints on dust-obscured star formation in high-z galaxies, which can be obtained with new ALMA and future JWST observations.

Appendix A: Fits for the [C II]–SFR relation at high redshift

The ALPINE dataset and the data for $z > 6$ galaxies from the literature have been fitted using a Bayesian fit including censored data following the method of Kelly (2007), which is implemented in the *linmix* python package. In Table A.1 we list the resulting fit coefficients of the linear fits of the form $\log(L([\mathrm{CII}])/L_\odot) = a + b \times \log(\mathrm{SFR_{tot}}/M_\odot \mathrm{yr}^{-1})$ and their uncertainties obtained for different combinations of datasets, assumptions on SFR(tot), and adopted [C II] upper limits. Not all combinations are shown and discussed in the text; those shown in Figures are indicated by the last column in the table.

Acknowledgements. This paper is based on data obtained with the ALMA Observatory, under Large Program 2017.1.00428.L. ALMA is a partnership of ESO (representing its member states), NSF(USA) and NINS (Japan), together with NRC (Canada), MOST and ASIAA (Taiwan), and KASI (Republic of Korea), in cooperation with the Republic of Chile. The Joint ALMA Observatory is operated by ESO, AUI/NRAO and NAOJ. DS, MG and MD acknowledge support from the Swiss National Science Foundation. AC, CG, FL, FP and MT acknowledge the support from grant PRIN MIUR 2017 - 20173ML3WW_001. EI acknowledges partial support from FONDECYT through grant N° 1171710. GCJ and RM acknowledge ERC Advanced Grant 695671 "QUENCH" and support by the Science and Technology Facilities Council (STFC). DR acknowledges support from the National Science Foundation under grant numbers AST-1614213 and AST-1910107 and from the Alexander von Humboldt Foundation through a Humboldt Research Fellowship for Experienced Researchers. ST acknowledges support from the ERC Consolidator Grant funding scheme (project ConTExT, grant No. 648179). The Cosmic DAWN Center is funded by the Danish National Research Foundation under grant No. 140 LV acknowledges funding from the European Union's Horizon 2020 research and innovation program under the Marie Sklodowska-Curie Grant agreement No. 746119.

References

Arata, S., Yajima, H., Nagamine, K., Abe, M., & Khochfar, S. 2020, arXiv e-prints, arXiv:2001.01853
Bakx, T. J. L. C., Tamura, Y., Hashimoto, T., et al. 2020, arXiv e-prints, arXiv:2001.02812
Bouwens, R. J., Aravena, M., Decarli, R., et al. 2016, ApJ, 833, 72
Bradač, M., Garcia-Appadoo, D., Huang, K.-H., et al. 2017, ApJL, 836, L2
Capak, P. L., Carilli, C., Jones, G., et al. 2015, Nature, 522, 455
Carilli, C., Murphy, E., Ferrara, A., & Dayal, P. 2017
Carniani, S., Maiolino, R., Amorin, R., et al. 2018, MNRAS, 478, 1170
Chabrier, G. 2003, PASP, 115, 763
de Looze, I., Baes, M., Bendo, G. J., Cortese, L., & Fritz, J. 2011, MNRAS, 416, 2712
De Looze, I., Cormier, D., Lebouteiller, V., et al. 2014, A&A, 568, A62
Diaz-Santos, T., Armus, L., Charmandaris, V., et al. 2013, ApJ, 774, 68
Faisst, A. L., Capak, P. L., Yan, L., et al. 2017, ApJ, 847, 21
Faisst, A. L., Schaerer, D., Lemaux, B. C., et al. 2019, arXiv e-prints, arXiv:1912.01621
Ferrara, A., Hirashita, H., Ouchi, M., & Fujimoto, S. 2017, MNRAS, 471, 5018
Ferrara, A., Vallini, L., Pallottini, A., et al. 2019, MNRAS, 489, 1
Graciá-Carpio, J., Sturm, E., Hailey-Dunsheath, S., et al. 2011, ApJL, 728, L7
Gullberg, B., De Breuck, C., Vieira, J. D., et al. 2015, MNRAS, 449, 2883
Harikane, Y., Ouchi, M., Inoue, A. K., et al. 2019, arXiv e-prints, arXiv:1910.10927
Harikane, Y., Ouchi, M., Shibuya, T., et al. 2018, The Astrophysical Journal, 859, 84
Hashimoto, T., Laporte, N., Mawatari, K., et al. 2018, Nature, 557, 392
Hirashita, H., Burgarella, D., & Bouwens, R. J. 2017
Hollenbach, D. J. & Tielens, A. G. G. M. 1999, Reviews of Modern Physics, 71, 173
Inoue, A. K., Tamura, Y., Matsuo, H., et al. 2016, Science, 352, 1559
Kelly, B. C. 2007, ApJ, 665, 1489
Kennicutt, Jr., R. C. 1998, ARA&A, 36, 189
Knudsen, K. K., Richard, J., Kneib, J.-P., et al. 2016, Monthly Notices of the Royal Astronomical Society: Letters, 462, L6
Kohandel, M., Pallottini, A., Ferrara, A., et al. 2019, MNRAS, 487, 3007
Lagache, G., Cousin, M., & Chatzikos, M. 2018, A&A, 609, A130
Laporte, N., Ellis, R. S., Boone, F., et al. 2017, ApJL, 837, L21
Laporte, N., Katz, H., Ellis, R. S., et al. 2019, MNRAS, 487, L81
Le Fèvre, O., Béthermin, M., Faisst, A., et al. 2019, arXiv e-prints, arXiv:1910.09517
Madau, P. & Dickinson, M. 2014, ARA&A, 52, 415
Maiolino, R., Carniani, S., Fontana, A., et al. 2015, MNRAS, 452, 54
Malhotra, S., Kaufman, M. J., Hollenbach, D., et al. 2001, ApJ, 561, 766
Marrone, D. P., Spilker, J. S., Hayward, C. C., et al. 2018, Nature, 553, 51
Matthee, J., Sobral, D., Boogaard, L. A., et al. 2019, ApJ, 881, 124
Murphy, E. J., Condon, J. J., Schinnerer, E., et al. 2011, ApJ, 737, 67
Ota, K., Walter, F., Ohta, K., et al. 2014, ApJ, 792, 34
Ouchi, M., Ellis, R., Ono, Y., et al. 2013, ApJ, 778, 102
Pentericci, L., Carniani, S., Castellano, M., et al. 2016, ApJL, 829, L11
Pineda, J. L., Langer, W. D., & Goldsmith, P. F. 2014, A&A, 570, A121
Popping, G., Narayanan, D., Somerville, R. S., Faisst, A. L., & Krumholz, M. R. 2019, MNRAS, 482, 4906
Riechers, D. A., Carilli, C. L., Capak, P. L., et al. 2014, ApJ, 796, 84
Schaerer, D., de Barros, S., & Sklias, P. 2013, A&A, 549, A4
Schreiber, C., Elbaz, D., Pannella, M., et al. 2018, A&A, 609, A30
Tamura, Y., Mawatari, K., Hashimoto, T., et al. 2019, ApJ, 874, 27
Vallini, L., Gallerani, S., Ferrara, A., Pallottini, A., & Yue, B. 2015, The Astrophysical Journal, 813, 36
Willott, C. J., Carilli, C. L., Wagg, J., & Wang, R. 2015, ApJ, 807, 180
Wolfire, M. G., Hollenbach, D., McKee, C. F., Tielens, A. G. G. M., & Bakes, E. L. O. 1995, ApJ, 443, 152
Wuyts, S., Förster Schreiber, N. M., Lutz, D., et al. 2011, ApJ, 738, 106
Zanella, A., Daddi, E., Magdis, G., et al. 2018, Monthly Notices of the Royal Astronomical Society, 481, 1976

Table A.1. Fit coefficients from Bayesian fits including censored data: (a, b)=(offset, slope) and their uncertainties (standard deviation). Col. 1 indicates the dataset used, col. 2 the total SFR used, col. 3 the [C II] limits. Col. 8 indicates the figure number showing the corresponding data and fit in some cases.

Dataset	SFR	[C II] limits	offset	std(offset)	slope	std(slope)	Fig.
ALPINE	UV+IR	3-σ limits	7.03	0.17	1.00	0.12	2
ALPINE	UV+IR	6-σ	7.37	0.14	0.83	0.10	
ALPINE	SED	3-σ	7.09	0.21	0.84	0.13	3 right
ALPINE	SED	6-σ	7.43	0.17	0.70	0.10	
ALPINE	UV+IRX	3-σ	6.59	0.20	1.17	0.12	4
ALPINE	UV+IRX	6-σ	6.98	0.16	0.99	0.09	5
ALPINE+$z > 6$	UV+IRX	3-σ	6.43	0.16	1.26	0.10	6
ALPINE+$z > 6$	UV+ (IRX for ALPINE only)	3-σ	6.50	0.16	1.22	0.10	
ALPINE+$z > 6$	UV+IRX	6-σ	6.66	0.14	1.16	0.08	

[1] Observatoire de Genève, Université de Genève, 51 Ch. des Maillettes, 1290 Versoix, Switzerland
[2] CNRS, IRAP, 14 Avenue E. Belin, 31400 Toulouse, France
[3] Aix Marseille Université, CNRS, CNES, LAM (Laboratoire d'Astrophysique de Marseille), 13013, Marseille, France
[4] IPAC, California Institute of Technology, 1200 East California Boulevard, Pasadena, CA 91125, USA
[5] Department of Physics, University of California, Davis, One Shields Ave., Davis, CA 95616, USA
[6] Dipartimento di Fisica e Astronomia, Università di Padova, Vicolo dell'Osservatorio, 3 35122 Padova, Italy
[7] INAF, Osservatorio Astronomico di Padova, vicolo dell'Osservatorio 5, I-35122 Padova, Italy
[8] Kavli Institute for the Physics and Mathematics of the Universe, The University of Tokyo, Kashiwa, Japan 277-8583 (Kavli IPMU, WPI)
[9] University of Bologna, Department of Physics and Astronomy (DIFA), Via Gobetti 93/2, I-40129, Bologna, Italy
[10] INAF - Osservatorio Astrofisico di Arcetri, Largo E. Fermi 5, I-50125, Firenze, Italy
[11] INAF - Osservatorio di Astrofisica e Scienza dello Spazio di Bologna, via Gobetti 93/3, I-40129, Bologna, Italy
[12] Instituto de Investigacion Multidisciplinar en Ciencia y Tecnologia, Universidad de La Serena, Raul Bitran 1305, La Serena, Chile
[13] Departamento de Astronomia, Universidad de La Serena, Av. Juan Cisternas 1200 Norte, La Serena, Chile
[14] Centro de Astronomia (CITEVA), Universidad de Antofagasta, Avenida Angamos 601, Antofagasta, Chile
[15] Cavendish Laboratory, University of Cambridge, 19 J. J. Thomson Ave., Cambridge CB3 0HE, UK
[16] Kavli Institute for Cosmology, University of Cambridge, Madingley Road, Cambridge CB3 0HA, UK
[17] Space Telescope Science Institute, 3700 San Martin Drive, Baltimore, MD 21218, USA
[18] European Southern Observatory, Av. Alonso de Córdova 3107, Vitacura, Santiago, Chile
[19] Astronomy Department, University of Massachusetts, Amherst, MA 01003, USA
[20] Instituto de Física y Astronomía, Universidad de Valparaíso, Avda. Gran Bretaña 1111, Valparaíso, Chile
[21] Leiden Observatory, Leiden University, PO Box 9500, 2300 RA Leiden, The Netherlands
[22] Max-Planck Institut für Astronomie, Königstuhl 17, D-69117, Heidelberg, Germany
[23] The Caltech Optical Observatories, California Institute of Technology, Pasadena, CA 91125, USA
[24] Waseda University, Department of Physics, Waseda Research Institute for Science and Engineering Tokyo, Japan
[25] Research Institute for Science and Engineering, Waseda University, 3-4-1 Okubo, Shinjuku, Tokyo 169-8555, Japan
[26] National Astronomical Observatory of Japan, 2-21-1, Osawa, Mitaka, Tokyo, Japan
[27] Cosmic Dawn Center (DAWN), Copenhagen, Denmark
[28] Niels Bohr Institute, University of Copenhagen, Lyngbyvej 2, DK-2100 Copenhagen, Denmark
[29] Department of Astronomy, Cornell University, Space Sciences Building, Ithaca, NY 14853, USA
[30] Department of Astronomy, University of Florida, 211 Bryant Space Sciences Center, Gainesville, FL 32611 USA
[31] University of Florida Informatics Institute, 432 Newell Drive, CISE